11th International Symposium on Turbulence and Shear Flow Phenomena (TSFP11)
Southampton, UK, July 30 to August 2, 2019

PERFORMANCE AND SCALING OF FLEXIBLE INERTIAL SWIMMERS

Daniel Floryan
Dept. of Mech. and Aero. Eng.
Princeton University
Princeton, NJ 08544, USA
dfloryan@princeton.edu

Tyler Van Buren
Dept. of Mech. and Aero. Eng.
Princeton University
Princeton, NJ 08544, USA
tburen@princeton.edu

Alexander J. Smits
Dept. of Mech. and Aero. Eng.
Princeton University
Princeton, NJ 08544, USA
asmits@princeton.edu

ABSTRACT

Experiments are described on the propulsive performance of flexible plates sinusoidally actuated at the leading edge and passively deforming along the chord. Local resonant boosts in deflection, thrust, and power appear as the plates are actuated near natural frequencies. Nonlinear finite-amplitude effects are evident, and, among other reasons, render scaling results from the literature ineffective. We use physical arguments to define new scaling variables, and show how they are able to capture the behaviour of the propulsive performance.

INTRODUCTION

An important quality of swimmers is the flexibility of their propulsive surfaces (for example, the caudal or tail fin). When a swimmer actuates its propulsor near a resonant frequency of the coupled fluid-structure system, the flexible propulsor may experience a boost in thrust (Alben, 2008) and efficiency (Dewey et al., 2013) compared to its rigid counterpart. Although conferring important propulsive benefits, the flexibility of the propulsor makes a simple analysis evasive.

To this end, we seek to develop scaling laws that provide meaningful physics responsible for the observed fluid-structure phenomena. Since our interests lie mainly in propulsion, we shall focus on the thrust that flexible propulsors produce, as well as how efficiently they produce thrust.

Robust scaling laws have already been successfully developed for rigid propulsors (Floryan et al., 2017; Van Buren et al., 2018b; Floryan et al., 2018; Floryan et al., 2019). These scaling laws, along with the analytical theories of Garrick (1937) and Lighthill (1971), underscore the importance of the flow at the trailing edge of the propulsor (Van Buren at al., 2018a). We hypothesize that the condition of the trailing edge will be equally important for flexible propulsors. To test our hypothesis, we have undertaken a large experimental campaign spanning different motion types, amplitudes, frequencies, and stiffnesses of flexible propulsors.

PROBLEM SETUP

We consider a nominally two-dimensional, thin, inextensible elastic plate of length c, span s, thickness d, density ρ_s, and flexural rigidity $B = EI$, where E is the Young's modulus and $I = sd^3/12$ is the second moment of area of the plate, undergoing heave and pitch oscillations about its leading edge. The motions are described by $h(t) = h_0 \sin(2\pi ft)$ and $\theta(t) = \theta_0 \sin(2\pi ft + \phi)$, respectively, where h_0 is the heave amplitude, θ_0 is the pitch amplitude, ϕ is the phase between the two motions, and f is the frequency of oscillation, and are sketched in figure 1. The foil moves horizontally at a constant speed U_∞ through a fluid of density ρ_f and viscosity μ, and the motion of the foil causes the surrounding fluid to impart forces onto it. We are chiefly concerned with the time-averaged thrust coefficient, C_T, produced by the foil, the power input coefficient, C_P, and the efficiency of the thrust production, $\eta = C_T/C_P$. Here,

$$C_T = \frac{\overline{F_x}}{\frac{1}{2}\rho_f U_\infty^2 sc}, \quad C_P = \frac{\overline{F_y\dot{h} + M\dot{\theta}}}{\frac{1}{2}\rho_f U_\infty^3 sc}, \tag{1}$$

where F_x is the force produced in the streamwise direction (the thrust), F_y is the force produced in the transverse direction, M is the moment about the leading edge, and the overbar denotes time-averaging. A set of dimensionless parameters describing the problem are the reduced frequency, $f^* = fc/U_\infty$, the dimensionless heave and pitch amplitudes, the phase between heave and pitch, the mass ratio $R = \rho_s d/\rho_f c$, and the stiffness ratio $S = Ed^3/\rho_f U_\infty^2 c^3$. The mass ratio is small for swimmers since they are thin and neutrally buoyant, so its effects can be ignored. Other common dimensionless inputs can be constructed from the aforementioned dimensionless parameters.

Since the plate is passively flexible, its deformation is unknown a priori. The motion of the trailing edge must therefore be measured, whereas for rigid plates it can be calculated from the actuation parameters. In particular, the

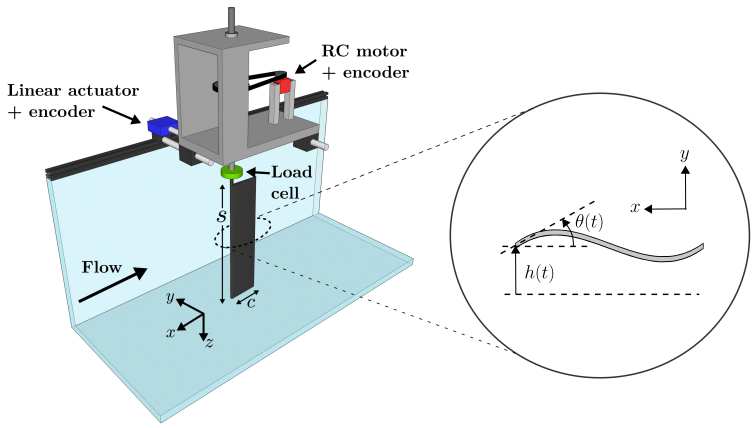

Figure 1. Experimental setup.

Strouhal number St cannot be calculated a priori, where

$$St = \frac{2fA_0}{U_\infty}. \tag{2}$$

Here, A_0 is the amplitude of the vertical displacement of the trailing edge.

Knowing the motion of the trailing edge is important because, as alluded to in the Introduction, it is a principal parameter governing the propulsive performance of flapping plates (at least rigid ones), although other parameters, such as f^*, are also important.

EXPERIMENTAL SETUP

We perform experiments on heaving and pitching plates in a water tunnel, shown schematically in figure 1. Rectangular plates of four different rigidities $B = 0.00136$, 0.00189, 0.00375, and 0.00736 N·m^2 are used, with a chord of $c = 124$ mm and span of $s = 180$ mm. Flat acrylic plates are installed at the top of the tunnel to eliminate surface waves. The tunnel velocity is fixed at $U_\infty = 100$ mm/s, yielding a chord-based Reynolds number of $Re = 12350$ and stiffness ratios $S = 4.77$, 6.64, 13.1, and 25.8. This range of stiffness ratios is outside of the range where flutter behaviour exists (Floryan & Rowley, 2018). Frequencies range between 0.2 and 1.5 Hz every 0.1 Hz, heave amplitudes are 0, 12.5, and 37.5 mm, and pitch amplitudes are 0°, 5°, and 15°. The reduced frequencies range between 0.284 and 1.86, and the dimensionless heave amplitudes are $h^* = h_0/c = 0$, 0.10, and 0.30. Forces and torques are measured directly via a six-component force and torque sensor, and heave and pitch at the leading edge are measured via encoders. Each case runs for 30 cycles of the motion, with the first and last five cycles used for warmup and cooldown. For each case, nine trials are performed; the plotted data in the rest of this work show quantities averaged across trials.

Measuring the position of the trailing edge presents a challenge. It is possible to record the motion of the flexible plate with a camera and extract the instantaneous shape of the plate from the recorded images. The sheer number of experiments, however, required a different approach. Here, we record the deflection of the plate at the mid-span at nine evenly spaced streamwise locations using a laser displacement sensor, massively reducing the amount of data taken and stored. Together with the encoder measurements, the laser displacement measurements are used to estimate the deflection of the plate.

Estimating the deflection

The laser displacement measurements at each location are passed through a Hampel filter in order to remove outliers and are then phase-averaged. The phase-averaged signal is smoothed in time by removing frequencies greater than the fifth harmonic of the actuation frequency. A cubic polynomial is fit to the filtered laser displacement and encoder measurements, yielding an estimate for the deflection

$$Y(x,t) = \sum_{n=0}^{3} c_n(t)x^n. \tag{3}$$

For the ranges of parameters explored in this study, a cubic polynomial has sufficient degrees of freedom to accurately model the deflection, but few enough degrees of freedom to avoid unphysical wiggliness. The coefficients c_0 and c_1 are fixed so that $Y(0,\cdot)$ is equal to the heave encoder measurements, and $Y_x(0,\cdot)$ is equal to the tangent of the pitch encoder measurements. The other coefficients are calculated by least squares regression. The coefficients c_n are then smoothed in time by removing frequencies greater than the third harmonic of the actuation frequency. The resulting polynomial accurately models the deflection between the leading edge and the location of the furthest downstream laser measurement.

Since the trailing edge lies downstream of the deflection measurement locations, we need to extrapolate to estimate its position. Most of the time, linear extrapolation is sufficient: we calculate the slope of the fitted polynomial at the furthest downstream laser measurement location, and extend a straight line with the same slope downstream until the arc length of the curve is equal to the length of the panel (the arc length of the polynomial is calculated by adaptive Gauss-Kronrod quadrature). We use this method for two reasons: (1) it satisfies the 'free-end' boundary conditions $\theta_s = \theta_{ss} = 0$ (no moment and no shear) at the trailing edge, where θ is the local angle of the plate and s is the arc length coordinate along the plate; and (2) it is robust to measurement noise. Linear extrapolation works well when the location of the furthest downstream laser measurement

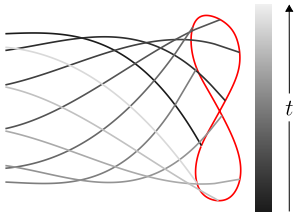

Figure 2. Ten snapshots, evenly spaced in time, of the deformation of a flexible heaving and pitching plate extracted from laser displacement measurements. The path of the trailing edge is shown as a red curve. Data corresponds to $f^* = 1.86$, $h^* = 0.302$, $\theta_0 = 15°$, $\phi = 270°$, and $S = 4.77$.

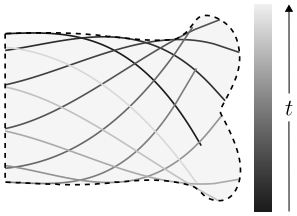

Figure 3. Same as figure 2, but showing the area swept by the plate.

is close to the trailing edge. At times, however, the panel deflects such that the trailing edge is upstream of the last laser measurement location. In this case, the next closest laser measurement may be relatively far from the trailing edge, and the panel may have significant curvature, making linear extrapolation inappropriate. When this happens, we instead find the unique quartic polynomial whose value, slope, and curvature match those of (3) at the location of the last valid laser measurement, that satisfies the free-end boundary conditions, and that yields the correct arc length. The location of the trailing edge must be iteratively solved for when using the quartic polynomial, and we use the previously described linear extrapolation method to provide an initial guess. Once the position of the trailing edge is calculated, it is smoothed in time by removing frequencies greater than the fifth (tenth) harmonic of the actuation frequency for the y (x) position of the trailing edge (the fundamental frequency of the x position of the trailing edge is twice the actuation frequency).

An alternative method is to estimate the local deflection angle θ as a function of the arc length coordinate s. We did so by estimating values of θ at the measurement locations by second-order finite difference, and values of s at the measurement locations by $\Delta s = \sqrt{\Delta x^2 + \Delta y^2}$, where Δx and Δy are the differences in the x and y coordinates between successive measurement locations. We then estimated θ as a polynomial in s, constraining it to satisfy the free-end boundary conditions at the trailing edge. The x and y coordinates are then calculated by integrating $\mathrm{d}x = \cos(\theta)\mathrm{d}s$ and $\mathrm{d}y = \sin(\theta)\mathrm{d}s$. Ultimately, we found this method to be sensitive to measurement noise, so all results reported here use the first method.

Figure 2 shows an example where we have extracted the shape of a flexible plate. The path of the trailing edge is drawn in red to highlight that we are able to extract the angle and velocity of the trailing edge. Although we have not done so in this example, we may enforce the up-down symmetry of the problem by only using the first few odd temporal Fourier modes of the shape. Since we have the entire deflection field of the plate, we may also calculate the area swept by the plate, as shown in figure 3.

RESULTS AND DISCUSSION

In figure 4, we plot the trailing edge amplitude relative to that of a rigid plate with the same leading edge actuation as a function of the reduced frequency. Here and throughout, darker curves correspond to stiffer plates. The curves all show peaks in amplitude, with stiffer plates having peaks at greater reduced frequencies.

As shown in Floryan & Rowley (2018), for large enough values of S, reduced frequencies corresponding to natural frequencies of the fluid-structure system scale as $\sqrt{S}$, so natural frequencies should occur at constant values of $f^*/\sqrt{S}$. This result is obtained by noting that for an Euler-Bernoulli beam in vacuum only one time scale exists, and in a fluid where the mass ratio is small the time scale is modified by replacing the characteristic solid mass by the characteristic fluid mass. The same dmensionless frequency was identified in Dewey et al. (2013) and Quinn et al. (2014) through different physical arguments. When replotting the trailing edge amplitude against this rescaled frequency, as in figure 5, we see that the peaks align. We also see that greater amplitudes of leading edge actuation reduce the natural frequency and the amplitude relative to that of a rigid plate. In a linear system, the curves for different amplitudes would collapse upon each other. The reductions in natural frequency and amplitude with increasing leading edge amplitude indicate that nonlinear, finite-amplitude effects are important in this system. Any scaling relations will have to reflect the nonlinearities present in the system, at least implicitly.

In figures 6 and 7, we show the thrust and power coefficients for our flexible plates scaled in such a way that, according to the literature, the data should collapse (Dewey et al., 2013; Quinn et al., 2014). In figure 7a, St_r is the same as the usual Strouhal number, but uses the trailing edge amplitude that a rigid plate with the same actuation would have. This scaling evidently does not work, and especially fails to capture amplitude effects in the case of pitching plates.

Since the thrust and power can be effectively scaled by the trailing edge velocity for rigid plates, we use the same concept here for flexible plates. In particular, we investigate three different Strouhal numbers for scaling the data. The first is St_r, which uses the trailing edge amplitude that would be achieved if the plate was rigid (we do not expect this to work since it does not capture any information about flexibility). The second is St as defined in (2) (it implicitly captures flexibility and nonlinear finite-amplitude effects since it uses the measured flexible trailing edge amplitude). Since St did not work for scaling the thrust of heaving plates, we define a third Strouhal number St_{sw}, which uses half of the area swept by the plate divided by the plate's length instead of A_0. The idea behind St_{sw} is that it captures how much fluid is put into motion by the plate.

The thrust and power of heaving and pitching plates are shown as functions of the three Strouhal numbers in figures 8–11. Not surprisingly, St_r is ineffective in all cases. St and St_{sw} fare better, especially for pitching plates, but even in those cases the data are somewhat spread apart (the data are more spread at lower Strouhal numbers, which is obscured by the scales of the vertical axes). For flexible plates, it is clear that the behaviour of the thrust and power cannot be simply captured by the behaviour of the trailing

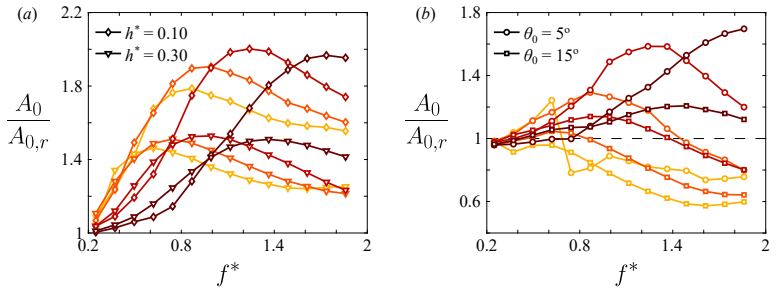

Figure 4. Ratio of trailing edge amplitude to that of a rigid plate with the same leading edge motion for (a) heaving and (b) pitching plates as a function of reduced frequency. Darker lines correspond to stiffer plates.

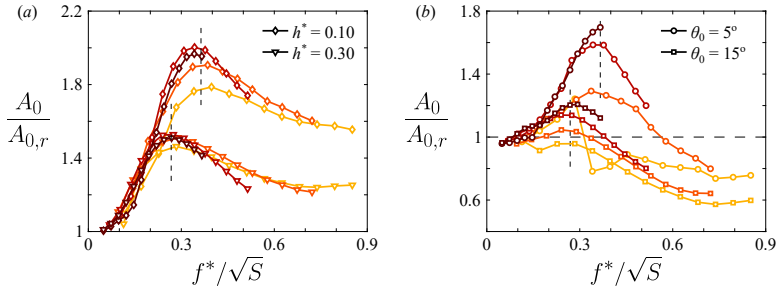

Figure 5. Same as figure 4, but as a function of a different dimensionless frequency.

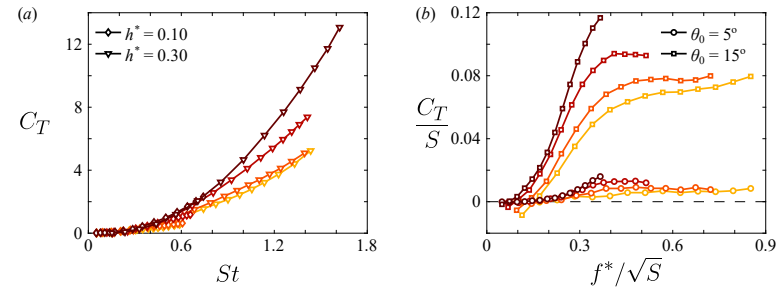

Figure 6. Thrust coefficient for (a) heaving plates using the scaling of Quinn et al. (2014), and (b) pitching plates using the scaling of Dewey et al. (2013).

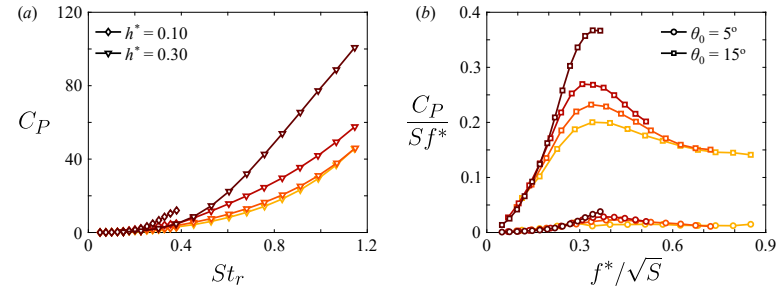

Figure 7. Power coefficient for (a) heaving plates using the scaling of Quinn et al. (2014), and (b) pitching plates using the scaling of Dewey et al. (2013).

edge as in the case of rigid plates.

We also show the efficiency as a function of the three Strouhal numbers for heaving and pitching plates in figures 12 and 13. As for thrust and power, the Strouhal numbers do not capture the behaviour of the efficiency. Plotting the efficiency as a function of the frequency that captured resonant behaviour does reveal some interesting tendencies, however, and is shown in figure 14. Two trends stand out: first, more flexible plates have greater efficiency; and second, smaller leading edge amplitudes have greater efficiency. More flexible plates may be more efficient because they offer less resistance against the preferred motion of the fluid, although this argument would also imply that they are less able to generate thrust. Greater amplitudes are likely less efficient because they produce greater offset drag (Floryan et al., 2018). That is, plates with greater amplitudes will have greater projected frontal areas, which increases the offset drag (the drag in the limit of vanishing frequency). For flexible plates, the offset drag cannot be determined directly because as the frequency decreases the dynamics of the deflection of the plate change, so the projected frontal area will as well.

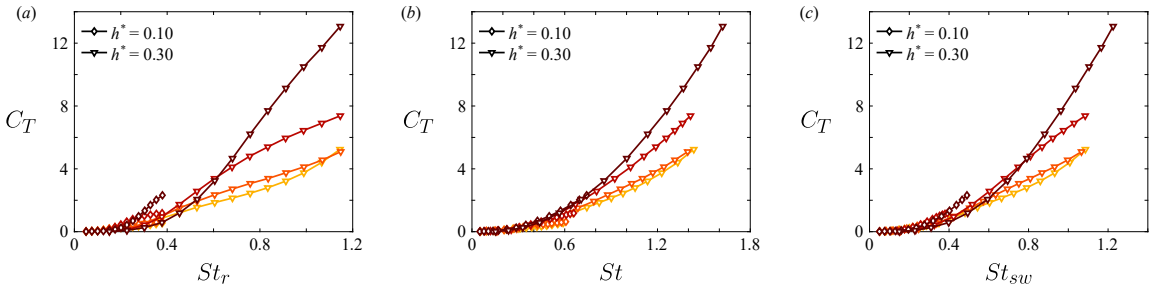

Figure 8. Thrust coefficient for heaving plates as a function of the Strouhal number based on (a) input amplitude, (b) measured amplitude, and (c) swept area.

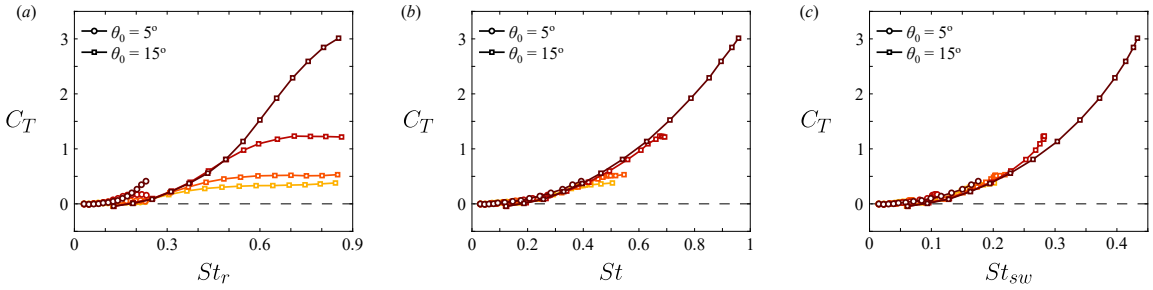

Figure 9. Thrust coefficient for pitching plates as a function of the Strouhal number based on (a) input amplitude, (b) measured amplitude, and (c) swept area.

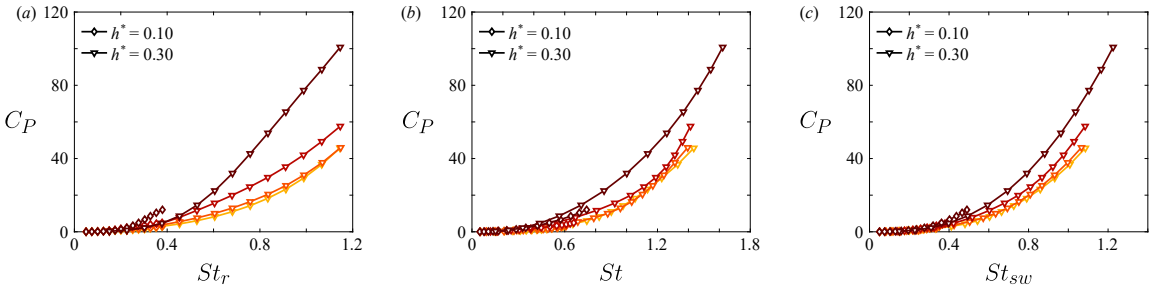

Figure 10. Power coefficient for heaving plates as a function of the Strouhal number based on (a) input amplitude, (b) measured amplitude, and (c) swept area.

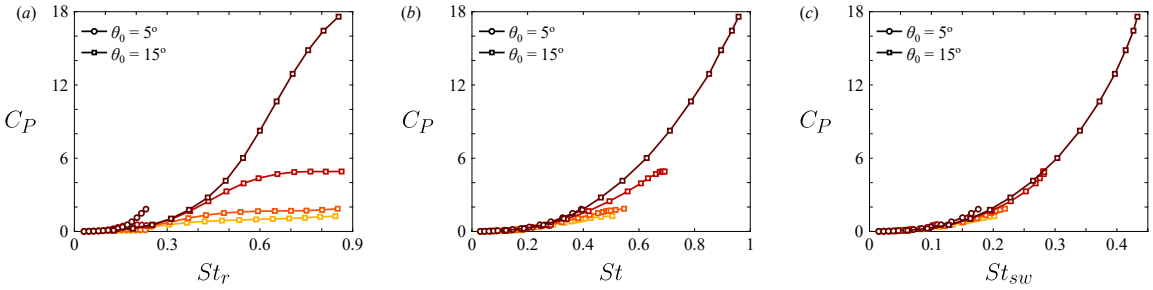

Figure 11. Power coefficient for heaving plates as a function of the Strouhal number based on (a) input amplitude, (b) measured amplitude, and (c) swept pitching.

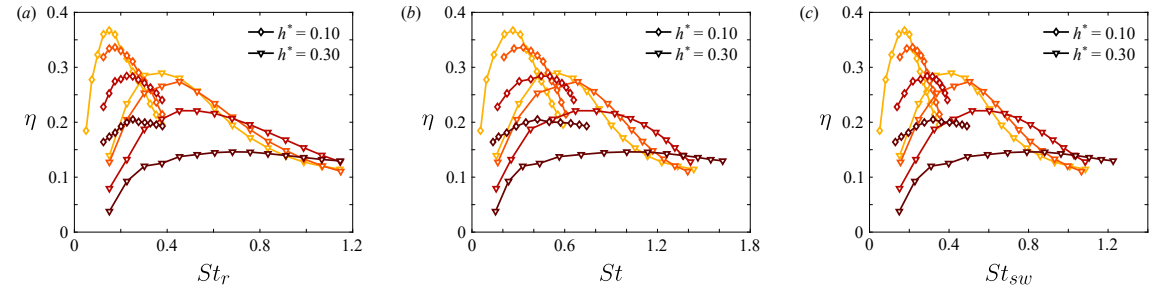

Figure 12. Efficiency for heaving plates as a function of the Strouhal number based on (a) input amplitude, (b) measured amplitude, and (c) swept area.

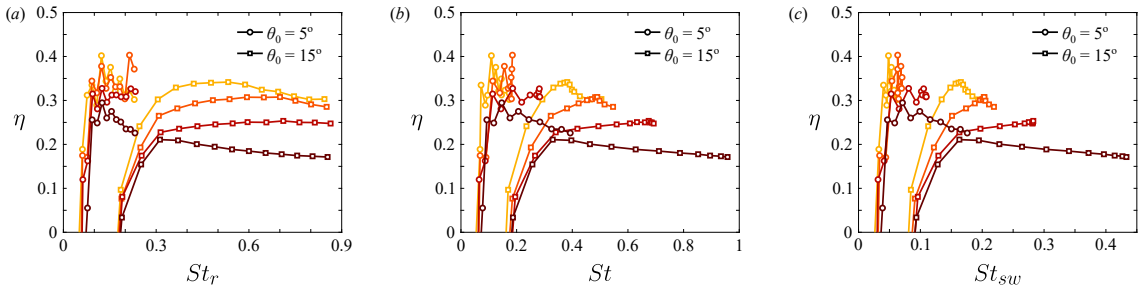

Figure 13. Efficiency for pitching plates as a function of the Strouhal number based on (a) input amplitude, (b) measured amplitude, and (c) swept area.

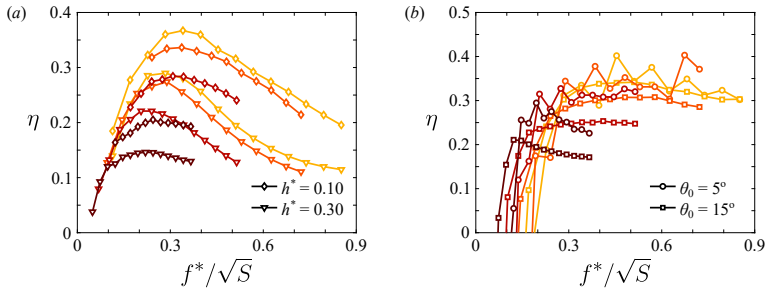

Figure 14. Efficiency for (a) heaving and (b) pitching plates as a function of the rescaled frequency used in figure 5.

CONCLUSIONS

We have described experiments on flapping flexible plates spanning different motion types, amplitudes, frequencies, and stiffnesses. For the ranges of frequencies and stiffnesses explored here, only the first resonant frequencies were observed. The flexible plates experience local boosts in thrust and power when actuated near a natural frequency, although the boosts are weak due to the natural frequencies being heavily damped. The efficiencies of the flexible plates have local peaks, as in the case of a rigid plate, but resonance modifies the frequency at which peak efficiency is attained. Nonlinear finite-amplitude effects are clearly important in the experiments.

As suggested by analytical results and experiments on rigid plates, the condition of the trailing edge is a vital factor in determining propulsive performance. In order to see if this result rings true for flexible plates, we have developed a novel low-cost method to accurately reconstruct the deflection of a flapping flexible plate, in particular the deflection of the trailing edge. We found that the condition of the trailing edge alone cannot capture the behaviour of thrust and power, although it seems to capture resonant phenomena. Simple scaling relations for the propulsive performance of flexible plates remain elusive.

This work was supported under ONR MURI grant N00014-14-1-0533 (Program Manager Robert Brizzolara).

REFERENCES

Alben, S., 2008, "Optimal flexibility of a flapping appendage in an inviscid fluid," Journal of Fluid Mechanics, Vol. 614, pp. 355–380.

Dewey, P. A., Boschitsch, B. M., Moored, K. W., Stone, H. A., and Smits, A. J., 2013, "Scaling laws for the thrust production of flexible pitching panels," Journal of Fluid Mechanics, Vol. 732, pp. 29–46.

Floryan, D., Van Buren, T., Rowley, C. W., and Smits, A. J., 2017, "Scaling the propulsive performance of heaving and pitching foils," Journal of Fluid Mechanics, Vol. 822, pp. 286–397.

Floryan, D., and Rowley, C. W., 2018, "Clarifying the relationship between efficiency and resonance for flexible inertial swimmers," Journal of Fluid Mechanics, Vol. 853, pp. 271–300.

Floryan, D., Van Buren, T., and Smits, A. J., 2018, "Efficient cruising for swimming and flying animals is dictated by fluid drag," Proceedings of the National Academy of Sciences, Vol. 115(32), pp. 8116–8118.

Floryan, D., Van Buren, T., and Smits, A. J., 2019, "Large-amplitude oscillations of foils for efficient propulsion," under review.

Garrick, I. E., 1937, "Propulsion of a flapping and oscillating foil." NACA Technical Report 567.

Lighthill, M. J., 1971, "Large-amplitude elongated-body theory of fish locomotion," Proceedings of the Royal Society B, Vol. 179(1055), pp. 125–138.

Quinn, D. B., Lauder, G. V., and Smits, A. J., 2014, "Scaling the propulsive performance of heaving flexible panels," Journal of Fluid Mechanics, Vol. 738, pp. 250–267.

Van Buren, T., Floryan, D., Wei, N., and Smits, A. J., 2018a, "Flow speed has little impact on propulsive characteristics of oscillating foils," Physical Review Fluids, Vol. 3(1), pp. 013103.

Van Buren, T., Floryan, D., and Smits, A. J., 2018b, "Scaling and performance of simultaneously heaving and pitching foils," AIAA Journal, online.